A FULL ORBIT XMM-NEWTON OBSERVATION OF PKS 2155-304

Laura Maraschi[1], Fabrizio Tavecchio[1], Ilaria Cagnoni[2], You-Hong Zhang[2], Lucio Chiappetti[3], Aldo Treves[2], Annalisa Celotti[4], Luigi Costamante[5], Rick Edelson[6,7], Giovanni Fossati[8], Gabriele Ghisellini[5], Elena Pian[9], Steve Sembay[7], Gianpiero Tagliaferri[5], and C. Megan Urry[10]

[1]Osservatorio Astronomico di Brera, Via Brera 28 I-20121 Milano, Italy
[2]Dipartmento di Scienze, Università dell'Insubria, via Valleggio 11 Como, I-22100, Italy
[3]Instituto di Fisica Cosmica G. Occhialini, via Bassini 15, Milano, I-20133, Italy
[4]SISSA/ISAS, via Beirut 2-4 Trieste, I-34014, Italy
[5]Osservatorio Astronomico di Brera, via Bianchi 46 Merate, I-23807, Italy
[6]Astronomy Department, University of California, Los Angeles, CA 90095-1562, USA
[7]X-Ray Astronomy Group, University of Leicester, Leicester LE1 7RH, UK
[8]Dept. of Physics and Astronomy, MS 108, 6100 Main street, Houston, TX, 77005 USA
[9]Osservatorio Astronomico di Trieste, via G. B. Tiepolo 11, Trieste, I-34131, Italy
[10]Yale Center for Astronomy & Astrophysics, PO Box 208121, New Haven CT 06520-8121, USA

Abstract

XMM observed the BL Lac PKS 2155-304 for a full orbit (∼150 ksec) on 2000 November 19-21. Preliminary results on the temporal and spectral analysis of data from the EPIC PN camera and Optical Monitor are presented. The variability amplitude depends systematically on energy, however the slopes of the structure functions of the light-curves in different bands do not appear to be significantly different. No evidence of time lags is found by cross correlating the light-curves in different bands.

Key words: BL Lacertae objects: general - BL Lacertae objects: individual (PKS 2155-304) - galaxies: active - X-rays galaxies

1. Introduction

Emission from Blazars is dominated by the non-thermal continuum produced in a relativistic jet pointing close to the line of sight (e.g. Urry & Padovani 1995). Thanks to the effects of relativistic beaming the jet flux can be enhanced by several orders of magnitude and its variability can therefore be studied observationally down to short timscales. Blazars hold crucial information on the physical processes taking place in relativistic jets. The "double humped" shape of the Spectral Energy Distribution (SED) is generally interpreted as due to synchrotron and Inverse Compton emission from a population of relativistic electrons in the jet. In fact from modelling the shape of the SED and the correlated variability of the two components it is possible to constrain the basic physical quantities of the jet (e.g. Sikora & Madejski 2001; Tavecchio et al. 1998). In particular, variability allows one to explore the acceleration and cooling processes acting on electrons. On this regard, especially valuable are observations in X-rays, which are produced by high-energy, fast-evolving particles.

Thanks to the *ASCA* and *Beppo-SAX* satellites, time lags between variability at different X-ray energies were discovered in PKS 2155-304 and Mkn 421. In the case of PKS 2155-304 lags were always of the same sign, soft X-rays lagging the harder ones, while both signs were found in Mkn 421. The simplest interpretation of these findings is that the emission from different X-ray energy bands is due to the same population of electrons. Within this picture the observed lags correspond to the time needed by the electrons to cool (soft lag) or accelerate (hard lag) and emit radiation in another energy band.

The main limitation to the *ASCA* and *Beppo-SAX* studies is related to the low orbit of such satellites: the periodic earth blockage prevents a continuous sampling of flux behaviuours, making temporal analysis more complicated and less reliable. The advent of the new generation satellites, such as *XMM-Newton* and *Chandra*, thanks to their high altitude and elliptical orbits, opens a new era in variability studies. In fact they offer continuous target visibility for up to about 40 hours compared with only ∼ 90 minutes from the low orbit satellites. In particular the big improvement offered by *XMM-Newton* is due to the combination of such a long continuous coverage of the target coupled with an unprecedently large effective area. Another striking feature of *XMM-Newton* is the possibility offered by the Optical Monitor to explore simultaneously the optical-UV bands.

With the goal of characterizing in a better way the variability we obtained a ∼ 150 ks *XMM-Newton* observation of one of the X-ray and UV brightest Blazars: PKS 2155-304.

PKS 2155-304 ($z = 0.116$) is a well known BL Lac object (a subclass class of blazars with an almost featureless optical spectrum), intensively monitored in the past years. Limiting quotations to results based on *ASCA*, *BeppoSAX*, *CHANDRA* or *XMM-Newton*, a minimal list of references is the following: Urry et al. 1997 (reporting simultaneous *ASCA*, *EUVE* and *IUE* lightcurves); Tanihata et al. 2001 (continuous 10-days *ASCA* observation); Kataoka et al. 2001 (summary of *ASCA* and *Rossi-XTE* lightcurves); Zhang et al. 2002 (summary of *BeppoSAX*

Proc. Symposium *'New Visions of the X-ray Universe in the XMM-Newton and Chandra Era'* 26–30 November 2001,

lightcurves); Nicastro et al. 2002 (the first spectrum of PKS 2155-304 obtained with the *Chandra* gratings). Edelson et al. (2001) report on a 100 ks-long *XMM-Newton* observation secured on May 30 2000 during the Performance Verification/Guaranteed Time Observation phase.

We present the results of a preliminary analysis of a long XMM-Newton pointing of PKS 2155-304 on Nov 19-21 2000. Due to problems in the satellite data analysis pipeline, the preprocessed data became available to us only recently. We present in this paper a preliminary analysis of the data of the EPIC PN camera and of the Optical Monitor (OM) only. EPIC MOS1 and MOS2 and RGS data will be discussed elsewhere (however see Brinkmann et al. in these proceedings).

2. Results

2.1. Data Analysis

PKS 2155-304 was observed during two uninterrupted pointings from Nov 19 (18:47:00 UT) to Nov 20 (10:47:49 UT) and from Nov 20 (13:01:39 UT) to Nov 21 (05:17:28 UT), respectively. The gap between the two parts is ∼2 hrs.

In order to avoid pile-up effects due to the large flux of the source, the PN camera was operated in the Small Window mode and the two MOS cameras in Timing Mode (MOS1) and Small Window Mode (MOS2). The data, processed with the standard pipeline, were analyzed with the *XMM-Newton Science Analysis System* (version 5.2.0).

A well known problem in EPIC data analysis is the background stability (e.g. Katayama et al. 2002). The background spectrum is dominated by particle events above 5 keV (e.g. Katayama et al. 2002). PKS 2155-304 emits most of its photons in the soft X-ray band so we were able to assess the stability of the background using a 1000 s binned light curve from events between 10 and 12 keV in a circular region ($r = 100''$) far from the source position (Figure 1 top). The first part of the observation has a stable background (with a mean of 10 counts per bin), while the second part shows changes ∼ 8 times larger than the quiescent level of ∼ 9.6 counts per bin. We conservatively excluded all the time intervals of the second part of the observation with background (10-12 keV) counts per bin larger than 13 (red line in Figure 1).

We extracted light curves in 3 energy bands, 0.1–2 keV, 2–4 keV and 4–10 keV with a bin size of 1000 s in a circular region with $r = 40''$ centered on the source position. Due to a visible trend of increasing source flux after the end of a consistent ($\geq$ 22 counts per bin) background flare (e.g. at time ∼ 1.83 and ∼ 1.9 in Figure 1), we conservatively excluded 3 more data points (i.e. 3000 s) after the end of such flares. The cleaned PN lightcurves normalized to their mean are presented in Figure 2 (colored points).

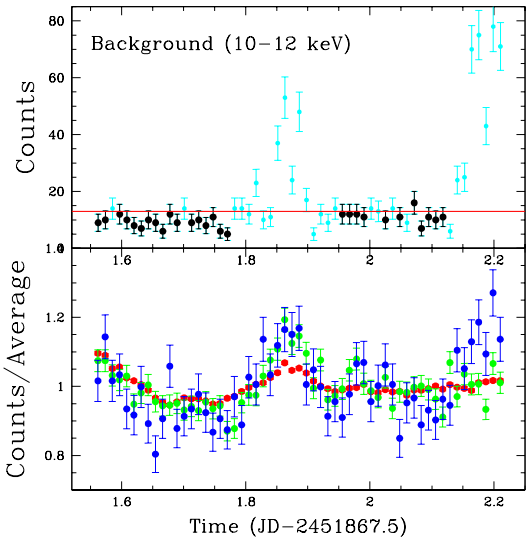

Figure 1. Background (top) and normalized EPIC PN (bottom) lightcurves of the second part of the observation. In the bottom panel red circles correspond to the 0.1–2 keV energy band, green the 2-4 keV and blue the 4-10 keV band. The red line in the top panel represents our cut: the cyan points represent the intervals of time we excluded.

PKS2155-304 has been also observed with the OM using the UVW2 filter (∼ 2000 Å). The OM was operated in the standard imaging mode, with exposure time frames of 800 s, giving an almost continuous coverage of the target. The source counts were extracted in a circular region with $r = 48''$ and the background in a concentric annular region from $48''$ to $2'$. The OM lightcurve normalized to the mean is shown in Figure 2 (black points).

Some simultaneous ground based photometry and polarimetry is available for the second part of the observation and will be presented elsewhere.

2.2. Temporal Analysis

To compare the amplitude of variability in the various energy bands we calculated the normalized excess variance, $\sigma^2_{\rm rms}$ (Zhang et al. 2002). This is given in Figure 3, which clearly shows that the trend of increased variability with energy found by e.g. Zhang et al. (2002), Edelson et al. (2001) in the X-ray regime extends to the UV. This trend is well modeled with a power law $\sigma^2_{\rm rms} = k \times (E/2.8284{\rm keV})^{\gamma}$ with $\gamma = 0.70$ and $k = 0.1070$.

2.2.1. Cross-correlation

To construct the cross-correlation function (CCF) we first normalized the light curves to zero mean and unit variance by subtracting the mean count rate and dividing by the

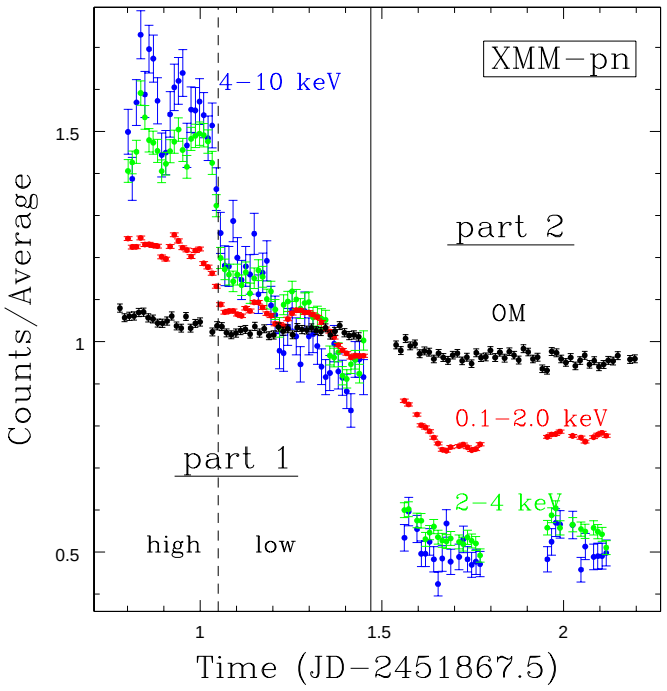

Figure 2. OM and EPIC PN lightcurves normalized to the mean. Black symbols represent OM data, red circles correspond to the 0.1–2 keV energy band, green the 2-4 keV and blue the 4-10 keV band.

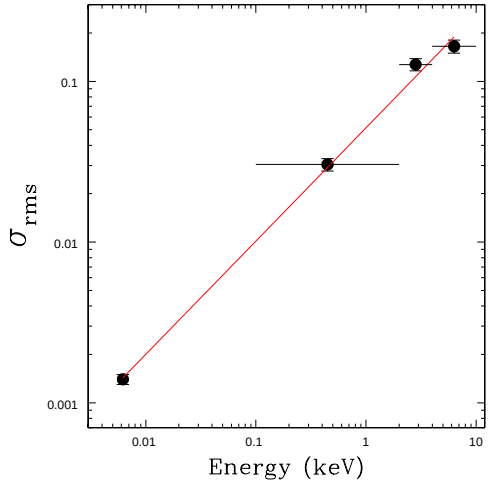

Figure 3. Normalized excess variance, $\sigma^2_{\rm rms}$, (as in Zhang et al. 2002) dependence on energy. The red line represents the best fit model.

rms (root mean squared) of the light curves (e.g., Edelson et al. 2001). The CCF is measured using the Discrete Correlation Function (DCF, Edelson & Krolik 1988). The bin size of the DCF is chosen to be 1200 s. We first calculated the DCFs of the first part of the observation which is the most variable during this campaign (see Figure 2). The DCF of the 0.1–2 keV versus the 4–10 keV energy bands shows that variability in these two bands is highly correlated, and, more important, there is no detectable time lag between the two bands. This behaviour is confirmed by the DCF analysis between other X-ray bands (i.e., 0.1–2 vs 2–4 keV, and 2–4 vs 4–10 keV). The DCF of the OM versus any of the PN energy bands for the first part of the observation shows an asymmetric structure at negative lags of still unclear nature, which disappears considering the whole observation.

2.2.2. Structure Function

We compute the Structure Function (SF) of each 1000 s binned lightcurve normalized to the square of the lightcurve mean, as in Zhang et al. (2002), so that the SFs can be directly compared. We subtract from each SF the contribution of the Poisson noise. The normalized SFs for the OM and for the 3 PN energy bands are shown in Figure 4.

As expected from the trend clearly visible in Figure 2 and Figure 3, the amplitude of the variability (i.e. the normalization of the SF curve) increases with the energy of the lightcurve.

We fit the normalized structure functions at times $> 10^4$ s (to exclude the region dominated by the Poisson noise) with a power law model: $SF(\tau) = k \times (\tau/20\text{ks})^{\beta}$. The best fit values for the normalization (k) and for the slope (β), together with their 1σ errors are reported in Table 1. A fit with a broken power law model suggests a break very close to the longest sampled timescales and does not improve the fit significantly.

Table 1. Fits to the normalized PN and OM structure functions assuming a power law model.

Energy band	β	k^a	χ^2/ν
OM	1.69 ± 0.71	0.620 ± 0.006	8.0
0.1–2 keV	1.44 ± 0.01	19.4 ± 1.4	26.6
2–4 keV	1.39 ± 0.01	86.8 ± 0.7	16.8
4–10 keV	1.41 ± 0.01	113.7 ± 10.8	12.2

[a] In units of 10^{-3}.

The large errorbars hide any possible dependence of the SF slope on the energy.

2.3. Spectral analysis

We divided the first part of the observation into two intervals: the "high" and "low" flux states (see Figure 2).

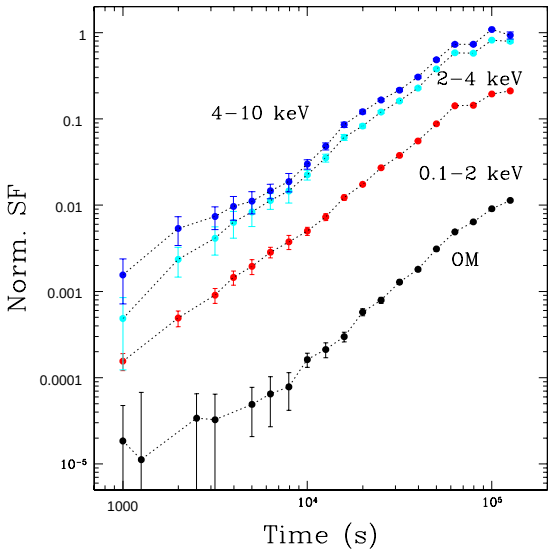

Figure 4. Normalized OM and PN (0.1–2 keV, 2–4 keV and 4–10 keV) structure functions (see text for details).

We present the first *XMM-Newton* EPIC spectrum of PKS2155-304. Due to unsolved problem of the calibration we restricted the analysis to the 0.6–10 keV energy range. We analyzed the spectral data using XSPEC (v.11) and the latest version of the response matrices (2001-12-11).

Table 2. Spectral fit to the high and low states of the first part of the observation assuming a broken power law model.

	Γ_1	Γ_2	E_b	χ^2/ν
High	2.73 ± 0.01	2.9 ± 0.1	4.6 ± 1.0	1.19
Low	2.82 ± 0.01	2.97 ± 0.05	3.6 ± 0.5	1.46

A simple (Galactic) absorbed power-law model is clearly inadequate to reproduce the spectrum. We then used the broken power-law model, which provides a good fit, except for an evident deficit of photons close to ~ 2.2 keV. This feature is located near to the Au instrumental edge in the telescope effective area and indicates residual uncertainties in the calibration at this energy in the SW mode.

The spectral indices measured in the high state ($\Gamma_1 = 2.73 \pm 0.01$ and $\Gamma_2 = 2.9 \pm 0.1$) indicate that the spectrum is steepening with energy. During the low state the data indicate a further significant steepening of the spectrum $\Gamma_1 = 2.82 \pm 0.01$ and $\Gamma_2 = 2.97 \pm 0.05$, consistent with what is usually observed in BL Lacertae objects (Urry et al. 1997; Kataoka et al. 2000). The 2–10 keV fluxes for the two states are 2.8×10^{-11} erg cm^{-2} s^{-1} and 2.03×10^{-11} erg cm^{-2} s^{-1}, respectively. PKS2155-304 is thus in a "low" state, similar to the 1996 *Beppo-SAX* observation (Giommi et al. 1998; Zhang et al. 2002).

The curved model of Fossati et al. (2000) does not improve the fit and t is not considered here.

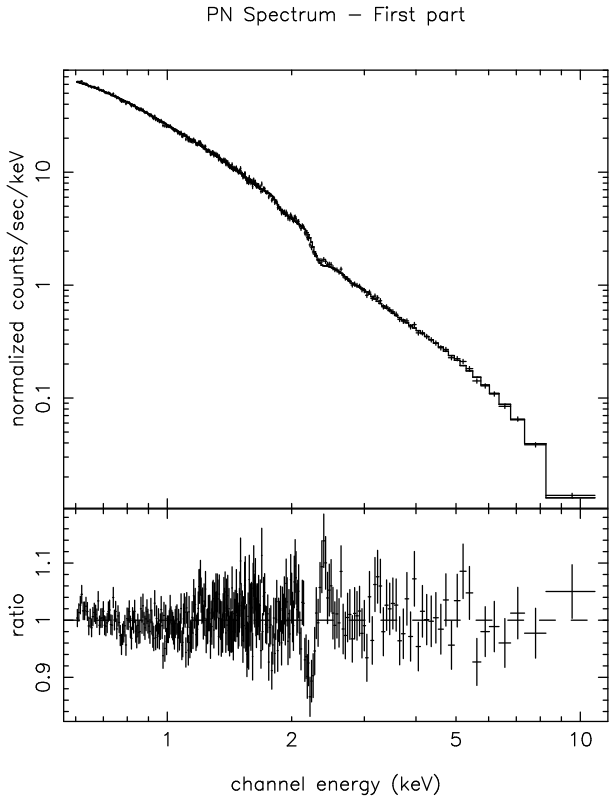

Figure 5. Energy spectrum of high state of the first part of the observation (top panel) and residuals to the fit (bottom panel). The feature at $\sim$ 2 keV is likely to be related to calibration uncertainties.

3. Discussion

During the observation the source was monotonically dimming with some superposed flickering. The most remarkable aspect is the energy dependence of the dimming, which is a factor 3 in 4–10 keV range and 20% in the UV (Figure 2 and 3). Figure 3 shows that variability increases regularly with the energy. Moreover the structure functions indicate that the dependence with the energy holds at all the timescales. Both results are consistent with the results of Edelson et al. (2001) and Zhang et al. (2002), but here are rather apparent, and are shown to extend to the UV range.

It is noticeable that in the presence of such a clear variability/energy dependence, the shape of the structure functions do not differ within the errors, indicating that the same variability mechanism is operating at all the in-

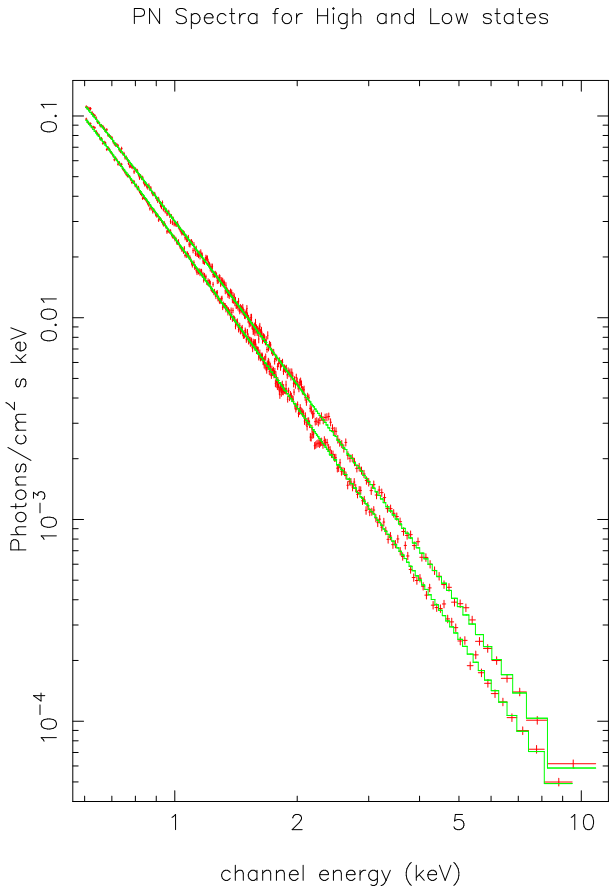

Figure 6. Unfolded spectra of high and low states of the first part of the the observation.

vestigated energies.

A further important point is the finding of no lags between different X-ray ranges. This is consistent with what reported by Edelson et al. (2001) in their *XMM-Newton* observation of PKS 2155-304, but it is an apparent disagreement with previous findings of time lags by the *ASCA* and *BeppoSAX* satellites (Kataoka et al. 2001; Tanihata et al. 2001; Zhang et al. 2002). It should be noted, however, that time lags have been found only in high-flux states, while both *XMM-Newton* observations found the source in a low state. Moreover, while during *ASCA* and *BeppoSAX* PKS 2155-304 was highly active and lightcurves included well defined flares, the *XMM-Newton* lightcurves are rather smooth, showing only slow variations. These differences could suggest that *variability is driven by different mechanisms in the low and the high state*. In order to assess this proposal, further observations in the X-ray/γ-ry domain are necessary.

Acknowledgements

We thank Valentina Braito for valuable help in the analysis of XMM data. We acknowledge support from Italian MUIR (contract COFIN MM02C71842) and ASI (grant I-R-105-00).

References

Edelson, R. A. & Krolik, J. H. 1988, ApJ, 333, 646

Edelson, R., Griffiths, G., Markowitz, A., Sembay, S., Turner, M. J. L., & Warwick, R. 2001, ApJ, 554, 274

Fossati, G. et al. 2000, ApJ, 541, 166

Giommi, P. et al. 1998, A&A, 333, L5

Kataoka, J., Takahashi, T., Makino, F., Inoue, S., Madejski, G. M., Tashiro, M., Urry, C. M., & Kubo, H. 2000, ApJ, 528, 243

Kataoka, J. et al. 2001, ApJ, 560, 659

Nicastro, F. et al. 2002, ApJ, in press (astro-ph/0201058).

Sikora, M. & Madejski, G. 2001, High Energy Gamma-Ray Astronomy, 275

Tanihata, C., Urry, C. M., Takahashi, T., Kataoka, J., Wagner, S. J., Madejski, G. M., Tashiro, M., & Kouda, M. 2001, ApJ, 563, 569

Tavecchio, F., Maraschi, L., & Ghisellini, G. 1998, ApJ, 509, 608

Urry, C. M. & Padovani, P. 1995, PASP, 107, 803

Urry, C. M. et al. 1997, ApJ, 486, 799

Zhang, Y.H., et al. 2002, ApJ, in press